Chinese Chemical Letters 35 (2024) 108845

Contents lists available at ScienceDirect

Chinese Chemical Letters

journal homepage: www.elsevier.com/locate/cclet

Interfacial assembly of 2D polydopamine/graphene heterostructures with well-defined mesopore and tunable thickness for high-energy planar micro-supercapacitors

Jieqiong Qin[a,*], Zhi Yang[a], Jiaxin Ma[b,c], Liangzhu Zhang[b], Feifei Xing[b,c], Hongtao Zhang[a], Shuxia Tian[d], Shuanghao Zheng[b], Zhong-Shuai Wu[b,*]

[a] College of Science, Henan Agricultural University, Zhengzhou 450002, China
[b] State Key Laboratory of Catalysis, Dalian Institute of Chemical Physics, Chinese Academy of Sciences, Dalian 116023, China
[c] University of Chinese Academy of Sciences, Beijing 100049, China
[d] Mechanical and Electrical Engineering Institute, Zhengzhou University of Light Industry, Zhengzhou 450002, China

ARTICLE INFO

Article history:
Received 11 June 2023
Revised 5 July 2023
Accepted 24 July 2023
Available online 26 July 2023

Keywords:
2D materials
Mesopores
Heterostructures
Polydopamine
High energy density
Micro-supercapacitors

ABSTRACT

Two-dimensional (2D) mesoporous pseudocapacitive polymer/graphene heterostructures combine the advanced merits of 2D materials and mesoporous materials, possessing unique nanosheet structure, large specific surface area (SSA), abundant oxygen/nitrogen-containing groups, desirable electrical conductivity and admirable electrochemical redox activity, and hold great potential for constructing high-performance planar micro-supercapacitors (MSCs). Herein, we demonstrate the interfacial assembly of 2D mesoporous polydopamine/graphene (mPDG) heterostructures with well-defined mesopore structure (12 nm) and adjustable thickness (7.5–14.1 nm) for planar high-energy pseudocapacitive MSCs. Attributed to medium thickness, exposed mesopore of 12 nm and large SSA of 108 m^2/g, the mPDG with 10.8 nm thickness reveals prominent mass capacitance of 419 F/g and impressive cycling stability with ~96% capacitance retention after 5000 cycles. Furthermore, the symmetric mPDG-based MSCs with "water-in-salt" gel electrolyte present wide voltage window of 1.6 V, superior volumetric energy density of 11.5 mWh/cm^3, outstanding flexibility and self-integration ability. Therefore, this work offers a new platform of controllably synthesizing 2D mesoporous heterostructures for high-performance MSCs.

With the continuously increasing requirement for portable and wireless electronic products, substantial endeavors have been devoted to developing flexible and reliable micro-electrochemical energy storage systems, mainly including micro-supercapacitors (MSCs) and micro-batteries [1–5]. Owing to the faster charge-discharge rate, longer cycle life and higher power density than micro-batteries, MSCs have garnered much attention [6–8]. To boost the energy density of MSCs, two-dimensional (2D) graphene-based heterostructures have been proved as one of promising active electrode materials [9–11]. They can effectively restrain the restacking of graphene and strongly couple with functional components, yielding satisfactory electrical conductivity, high electrochemical activity, rapid ion-electron transport and outstanding flexibility for MSCs. So far, various 2D heterostructures of carbon/graphene [12,13], metal oxide (hydroxide)/graphene [14–16], metal sulfide/graphene [17,18] and polymer/graphene [19–21] have been reported as active materials for MSCs, in which 2D pseudocapacitive polymer/graphene (*e.g.*, polypyrrole/graphene, polyaniline/graphene and polyethylene dioxythiophene/graphene) stands out because of fully integrating the high pseudocapacitance of polymer with extraordinary conductivity and flexibility of graphene.

By virtue of abundant oxygen/nitrogen-containing groups (*e.g.*, -OH, -COOH and -NH-), redox-active properties of catechol/ortho-quinone groups, unique adhesion and good biocompatibility, polydopamine (PDA) is considered as a high-pseudocapacitive material for surface modification of graphene (Fig. S1 in Supporting information) [22–25]. Through synergistically combining the high-conductive graphene and high-pseudocapacitive PDA, the resultant 2D PDA/graphene heterostructures have been widely used as active electrodes or functional protection materials of various metal-ion batteries [26–30]. However, their electrochemical and structural stability are severely hindered by the swell effect of PDA in charge-discharge process [23,30]. In this regard, the introduction of mesopore structure (2–50 nm) into 2D PDA/graphene will be an

* Corresponding authors.
E-mail addresses: qinjieqiong@henau.edu.cn (J. Qin), wuzs@dicp.ac.cn (Z.-S. Wu).

https://doi.org/10.1016/j.cclet.2023.108845
1001-8417/

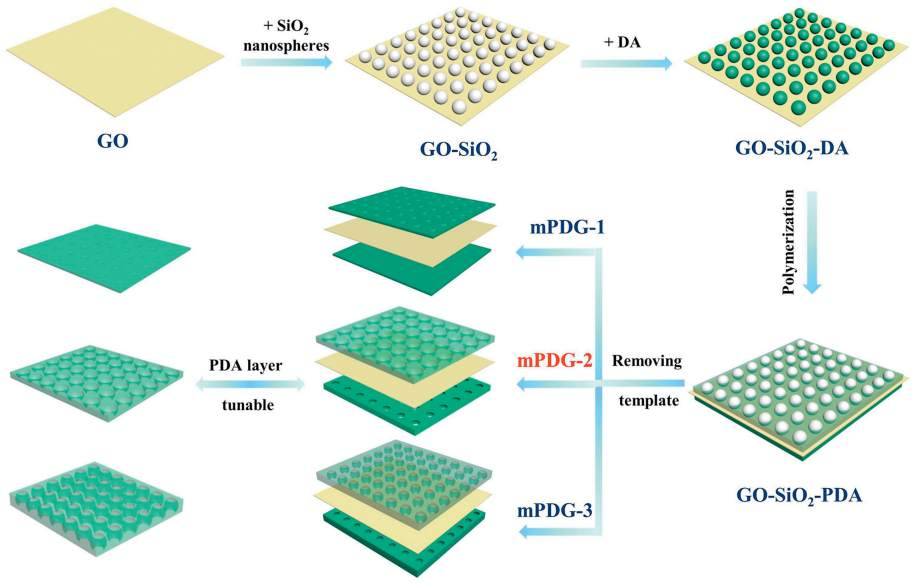

Fig. 1. Illustration of the fabrication of 2D mPDG heterostructures with tunable thickness and mesopore structure.

effective approach to provide increasing active sites, buffer the reversible volume changes, and enhance effective contact areas, ultimately realizing improved cycling stability as well as power and energy densities for MSCs [31–33]. Nonetheless, the precisely controllable assembly of 2D mesoporous PDA/graphene heterostructures for MSCs is underdeveloped so far.

Herein, we develop 2D mesoporous pseudocapacitive PDA/graphene (mPDG) heterostructures with well-defined mesopore structure and tunable thickness for high-energy planar MSCs. Using silica nanospheres as mesopore template and graphene oxide (GO) as 2D substrate, a series of mPDG heterostructures are successfully prepared by a dual-template interfacial assembly strategy. Remarkably, their sheet thickness can realize univariate regulation by precisely tailoring the amount of PDA monomer, which is of significance for elucidating their structure-activity relationship. Benefiting from medium thickness, exposed mesopore structure and larger specific surface area (SSA), mPDG with 10.8 nm thickness (mPDG-2) exhibits higher specific capacitance (419 F/g) and longer cycle life than mPDG with other thickness and non-mesoporous PDA/graphene (nPDG). Furthermore, mPDG-based MSCs with polyvinyl alcohol (PVA)-H_2SO_4 gel electrolyte (defined as mPDG-HMSCs) offer impressive volumetric capacitance of 34.3 F/cm^3 and energy density of 3.1 mWh/cm^3. What is more, mPDG-based MSCs with silica-lithium bis(trifluoromethane sulfonyl)imide (SiO_2-LiTFSI) gel electrolyte (mPDG-LMSCs) display high output voltage of 1.6 V and enhanced volumetric energy density of 11.5 mWh/cm^3. Finally, both mPDG-HMSCs and mPDG-LMSCs present good mechanical flexibility and facile self-integration, demonstrating their tremendous application potential in on-chip wearable microelectronics.

The fabrication of 2D mPDG heterostructures by a dual-template interfacial assembly strategy is displayed in Fig. 1. Specifically, GO nanosheets are firstly modified by polydiallyldimethylammonium chloride to produce positively-charged GO templates. Then, negatively charged SiO_2 nanospheres as mesopore templates are uniformly assembled on the modified GO surface according to their electrostatic interaction. Subsequently, dopamine (DA) monomers are added and adsorbed on the surface of GO-SiO_2 to form GO-SiO_2-DA composites. After initiating by tris(hydroxymethyl)aminomethane, the PDA layer is successfully polymerized and coated on GO-SiO_2, named as GO-SiO_2-PDA. Finally, 2D mPDG heterostructures are obtained by hydrothermal reduction and removing templates of SiO_2. Notably, the sheet thickness and mesopore structure of mPDG can be precisely regulated by changing the additive amount of DA monomers. With different amounts of DA (150, 300 and 600 mg), the resulting mPDG heterostructures are denoted as mPDG-1, mPDG-2 and mPDG-3, respectively.

The morphological and structural characterizations of 2D mPDG heterostructures are presented in Fig. 2 and Figs. S2-S4 (Supporting information). For mPDG-2, scanning electron microscope (SEM) image exhibits uniform and flat 2D morphology with exposed mesopore arrays (Fig. 2a). Transmission electron microscope (TEM) images further confirm the homogeneous mesopore structure with ~12 nm pore size (Figs. 2b and c). Meanwhile, mPDG-1 and mPDG-3 reveal unformed and partially encapsulated mesopores, respectively, deriving from the half and double amount of DA precursor compared with mPDG-2 (Fig. S2). Atomic force microscope (AFM) measurements confirm the varying thickness of 7.5 nm for mPDG-1, 10.8 nm for mPDG-2, and 14.1 nm for mPDG-3 (Figs. 2d and e, Fig. S3). In addition, their nitrogen adsorption-desorption isotherms display a typical H_3-type hysteresis loop, verifying the mesopore structure of mPDG (Fig. 2f and Fig. S4). The calculated SSA of mPDG-1, mPDG-2 and mPDG-3 is 80, 108 and 98 m^2/g, and the corresponding pore volume is 0.27, 0.38 and 0.34 cm^3/g, respectively. Moreover, it is observed that the mesopore diameter of mPDG-2 is ~10.7 nm, which is consistent with its TEM result. Consequently, it is demonstrated that dual-template interfacial assembly strategy can realize the precise regulation of sheet thickness and mesopore structure. Furthermore, X-ray photoelectron spectroscopy (XPS) measurement manifests the C, O and N elements in mPDG-2 (Fig. S5 in Supporting information) [23,28,29]. As shown in Fig. 2g, four peaks in the C 1s XPS spectrum are identified as C–C, C–O/C–N, C=O, and O–C=O at 284.7, 285.9, 288.0 and 290.6 eV, respectively [23,28,29]. The two primary peaks for the O 1s spectrum are 531.4 eV for O=C and 533.1 eV for O–C (Fig. 2h) [23,28,29]. The N 1s XPS spectrum exhibits three different binding energy from -N=, -NH- and -NH_2 at 398.9, 400.3 and 401.3 eV, respectively (Fig. 2i) [23,28,29]. The Fourier transform infrared spectroscopy (FTIR) spectrum of mPDG-2 exhibits distinct characteristics of PDA and graphene (Fig. S6 in Supporting information). The two feature peaks located at 2930 and 2850 cm^{-1} can be assigned

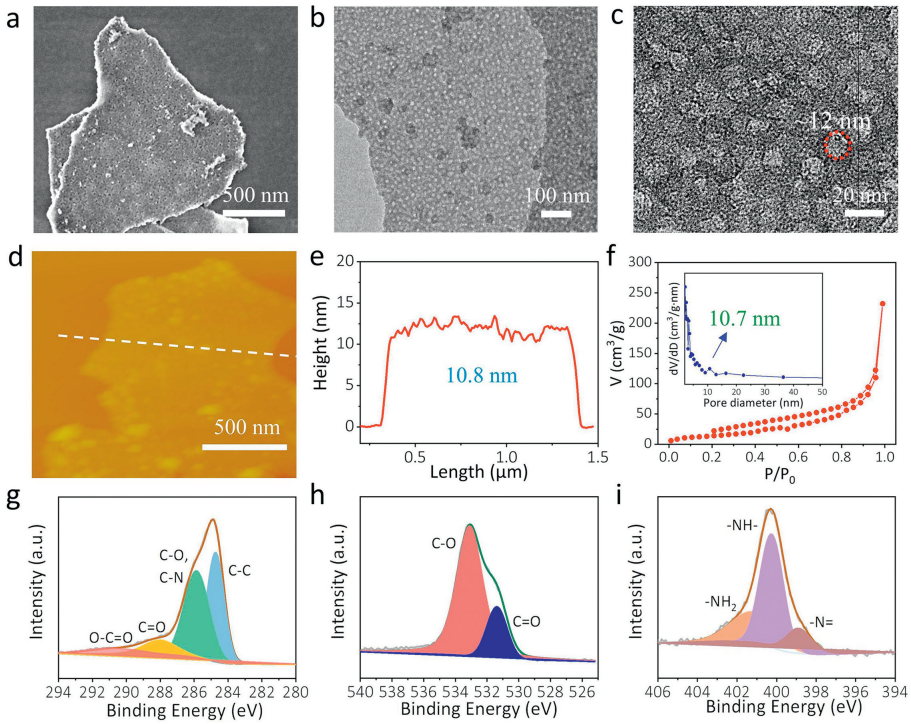

Fig. 2. Morphological and structural characterizations of 2D mPDG heterostructures. (a) SEM image, (b, c) TEM images, (d) AFM image and (e) corresponding height profile, (f) nitrogen adsorption-desorption isotherm and pore size distribution profile, (g) C 1s, (h) O 1s, and (i) N 1s XPS spectra of mPDG-2.

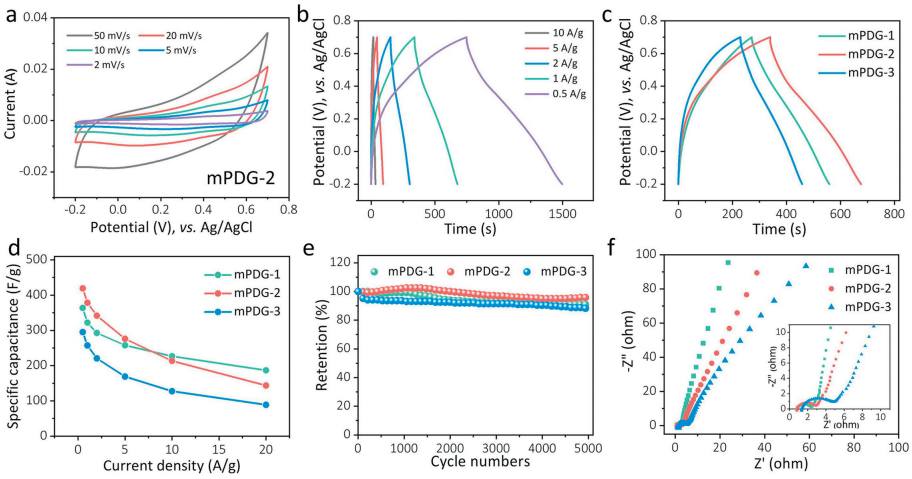

Fig. 3. Electrochemical performance of 2D mPDG working in a three-electrode system. (a) CV curves at 2–50 mV/s, and (b) GCD profiles at 0.5–10 A/g for mPDG-2. (c) GCD profiles measured at 1 A/g, (d) specific capacitances at varying current densities, (e) cycling stability over 5000 cycles at 1 A/g, and (f) EIS plots (inset: magnified high-frequency region) of mPDG-1, mPDG-2 and mPDG-3.

to the indole functional groups, the peak centered at 1460 cm^{-1} is induced by N–H [27,25], and the peak located at 1630 cm^{-1} is attributed to C=C in aromatic rings [34,35]. It is indicated that mPDG possesses abundant oxygen/nitrogen-containing groups, which is beneficial to provide high pseudocapacitance and excellent electrolyte wettability.

Because of uniform 2D morphology, adjustable mesopore structure, large SSA and abundant oxygen/nitrogen-containing groups, the mPDG heterostructures are expected to work as active materials for MSCs to achieve high performance. To demonstrate the impact of sheet thickness on electrochemical performance, mPDG-1, mPDG-2 and mPDG-3 are examined in H_2SO_4 electrolyte via a three-electrode system. In Figs. 3a and b, the cyclic voltammetry (CV) and galvanostatic charge discharge (GCD) profiles of mPDG-2 show pronounced pseudocapacitive behavior originating from redox-active PDA [25,36]. When the scan rate or current density increases, the CV curves and GCD profiles deliver incremental response current or discharge time, demonstrative of excellent electrochemical reversibility of mPDG. Compared with mPDG-1 and mPDG-3, the mPDG-2 presents a larger integral area at 50 mV/s and a longer discharge time at 1 A/g (Fig. S7 in Supporting information and Fig. 3c). Confirmed by Fig. 3d, mPDG-2 yields higher specific capacitance at 0.5–5 A/g than those of mPDG-1 and mPDG-3. Specifically, mPDG-2 reveals superior gravimetric capacitance of 419 F/g compared with mPDG-1 (363 F/g) and mPDG-3 (295 F/g) at 0.5 A/g. Furthermore, mPDG-2 can retain ~96% of initial capacitance over 5000 cycles, exceeding those of mPDG-1 (~91%) and mPDG-3 (~88%), which proves its better cycling stability derived

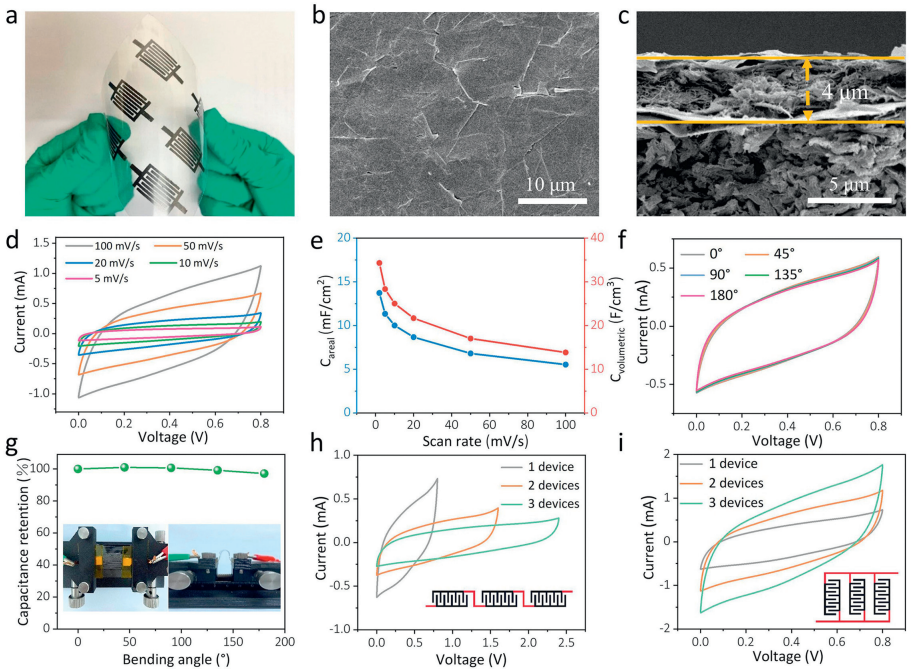

Fig. 4. Characterization and electrochemical performance of mPDG-HMSCs. (a) Photograph at a bending state, (b) top-view SEM image, and (c) cross-section SEM image of mPDG-based microelectrodes. (d) CV curves at 5–100 mV/s, (e) areal capacitance and volumetric capacitance *versus* scan rate of mPDG-HMSCs. (f) CV curves at 50 mV/s, and (g) capacitance retention of mPDG-HMSCs under varying bending angles of 0°–180° (insets: photographs of the device at 0° and 180°). (h, i) CV curves at 50 mV/s of three connected mPDG-HMSCs in (h) series and (i) parallel.

from fully exposed mesopore structure (Fig. 3e). The initial capacitance increase can be attributed to the electro-activation process of mPDG induced by the enhanced ion accessibility and increased charge accommodation in 2D mesoporous heterostructures during the long charge-discharge process [37–39]. Moreover, the mesopore structure endows mPDG-2 with a larger CV curve, longer discharge time, and thus much higher capacitance and rate performance than nPDG (Fig. S8 in Supporting information). Meanwhile, the nPDG presents only ~62% capacitance retention for 5000 cycles, which is far lower than mPDG-2, affirming that mesopore structure is able to alleviate the volume change of electrode materials in charge-discharge process. According to electrochemical impendence spectra (EIS), mPDG-2 reveals a measured internal resistance (R_s) of 0.8 Ω and the corresponding charge-transfer resistance (R_{ct}) of 2.1 Ω, which are lower than mPDG-3 ($R_s = 1.3$ Ω, $R_{ct} = 3.5$ Ω) and slightly higher than mPDG-1 ($R_s = 0.8$ Ω, $R_{ct} = 1.6$ Ω) (Fig. 3f). Similarly, the slope in low frequency of mPDG-2 is larger than mPDG-3 and less than mPDG-1, indicative of the advantage of thin sheet thickness and exposed mesopores for enhancing ion-electron transport.

Considering excellent performance merits, the mPDG-2 is selected as active electrode material for fabricating planar interdigital MSCs by a mask-assisted filtration technology [40–42], in which highly conductive exfoliated graphene (EG) is used as flexible metal-free current collector, and carbon nanotube (CNT) is applied as conductive additive to improve electrical conductivity of electrode. As exhibited in Fig. 4a, the interdigital microelectrodes display excellent uniformity and robust mechanical flexibility. The top and cross-section views clearly show a uniform and flat EG layer on the surface, and a sandwich-like layered structure with a thickness of ~4 μm (Figs. 4b and c, Fig. S9 in Supporting information). After drop-casting and solidifying PVA-H_2SO_4 electrolyte, the planar quasi-solid-state mPDG-HMSCs are obtained. Then, the CV curves of mPDG-HMSCs at 0–0.8 V display obvious pseudocapacitive feature and stepwise improved current with increasing scan rate (Fig. 4d). The GCD curves at 0.05–1 mA/cm^2 present similar shape and gradually increased charge-discharge times, indicating reversible electrochemical behavior of mPDG-HMSCs (Fig. S10 in Supporting information). Remarkably, mPDG-HMSCs deliver large areal capacitance and volumetric capacitance of 13.8 mF/cm^2 and 34.3 F/cm^3 at 2 mV/s, respectively (Fig. 4e), both of which surpass those of graphene/sulfonated polyaniline (rG/SPANI: 3.31 mF/cm^2, 16.55 F/cm^3) [43], laser-reduced GO (laser-rGO: 0.51 mF/cm^2, 3.1 F/cm^3) [44], rGO/CNT (5.1 mF/cm^2, 6.1 F/cm^3) [45] and laser-scribed graphene (LSG: 2.3 mF/cm^2, 3.1 F/cm^3) [46] based MSCs. The EIS plots of mPDG-HMSCs are shown in Fig. S11 (Supporting information). The mPDG-HMSCs also reveal impressive cycling stability of ~89% capacitance retention over 5000 cycles (Fig. S12 in Supporting information). Further, the mechanical flexibility and self-integration of mPDG-HMSCs were assessed to verify their potential applications in smart microelectronics. As shown in Figs. 4f and g, mPDG-HMSCs present nearly coincident CV curves under varying bending angles, showing ~97% retention at the bending angle of 180°. With continuous bending, mPDG-HMSCs can still maintain ~88% of initial capacitance for 1000 bending cycles, demonstrative of admirable mechanical flexibility (Fig. S13 in Supporting information). In addition, the CV curves and GCD profiles of three serially-connected mPDG-HMSCs illustrate similar shapes and stepwise voltage increase from 0.8 (one cell) to 2.4 V (three cells), as exhibited in Fig. 4h and Fig. S14 (Supporting information). Meanwhile, parallelly-connected mPDG-HMSCs display a linear increase of capacitance, verifying outstanding performance uniformity and accessible self-integration ability for high current/capacitance output (Fig. 4i and Fig. S15 in Supporting information).

According to the formula of $E = CV^2/2$, the energy density (E) of MSCs is directly proportional to specific capacitance (C) and the square of cell voltage (V) [47,48]. Thus, expanding the cell voltage with high-voltage electrolyte is a straightforward strategy to enhance the energy density of mPDG-based MSCs. To this purpose, a low-cost, highly safe SiO_2-LiTFSI "water-in-salt" (WIS) gel electrolyte was used to assemble high-voltage mPDG-LMSCs [42,49]. The CV curves and GCD profiles of mPDG-LMSCs verify a high voltage of 1.6 V (Fig. 5a and Fig. S16 in Supporting information) and

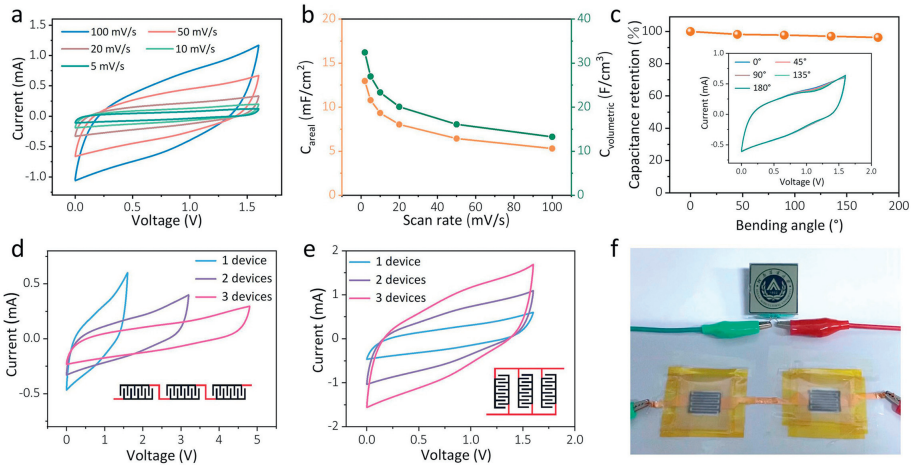

Fig. 5. Electrochemical performance of mPDG-LMSCs. (a) CV curves, (b) areal capacitance and volumetric capacitance *versus* scan rate of mPDG-LMSCs. (c) Capacitance retention *versus* bending angle for mPDG-LMSCs (Inset: CV curves at 50 mV/s). (d, e) CV curves of three connected mPDG-LMSCs in (d) series and (e) parallel. (f) Photograph of the logo of "Henan Agricultural University" powered by two serially-connected mPDG-LMSCs.

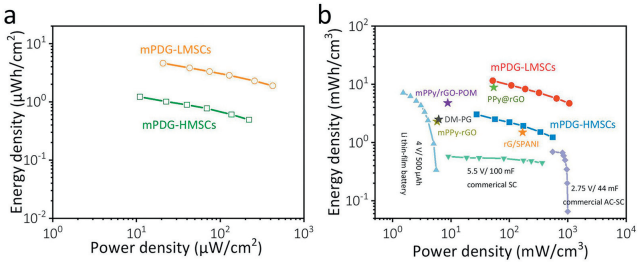

Fig. 6. Ragone plot of mPDG-HMSCs and mPDG-LMSCs. (a) Areal energy density and power density, and (b) volumetric energy density and power density of mPDG-HMSCs and mPDG-LMSCs with recently reported polymer/graphene-based MSCs and commercially available energy storage devices.

the EIS plots reveal low resistance (Fig. S17 in Supporting information). Notably, the areal capacitance and volumetric capacitance of mPDG-LMSCs are 12.9 mF/cm^2 and 32.4 F/cm^3, respectively (Fig. 5b). Besides, mPDG-LMSCs deliver impressive cycle stability of ~83% retention over 5000 cycles (Fig. S18 in Supporting information). With varying bending angles, mPDG-LMSCs present almost unchanged CV curves and ~96% capacitance retention even at 180°, demonstrative of superior mechanical flexibility (Fig. 5c). Further, serially-connected mPDG-LMSCs offer a progressive voltage expansion from 1.6 V for one cell to 4.8 V for three cells, while parallelly-connected mPDG-LMSCs disclose a stepwise current/capacitance increase, manifesting adjustable voltage and capacitance outputs (Figs. 5d and e, Figs. S19 and S20 in Supporting information). As demonstrated, two serially-connected mPDG-LMSCs can effectively drive a liquid crystal display with the logo of "Henan Agricultural University", and readily light up a red diode (Fig. 5f and Fig. S21 in Supporting information).

Further, the Ragone plot of mPDG-HMSCs and mPDG-LMSCs is provided to compare their energy density and power density with recently reported polymer/graphene-based MSCs (Figs. 6a and b). Expectedly, mPDG-LMSCs show the highest areal and volumetric energy densities of 4.6 μWh/cm^2 and 11.5 mWh/cm^3, which exceed those of mPDG-HMSCs (1.2 μWh/cm^2 and 3.1 mWh/cm^3). What is more, this value (11.5 mWh/cm^3) is considerably larger than other polymer/graphene-based MSCs, *e.g.*, rG/SPANI (1.5 mWh/cm^3) [43], mesoporous polypyrrole-rGO (mPPy-rGO: 2.3 mWh/cm^3) [50], mPPy/rGO anchored with polyoxometalate (mPPy/rGO-POM: 4.8 mWh/cm^3) [51], dual-mesoporous polypyrrole-graphene (DM-PG: 2.5 mWh/cm^3) [52] and polypyrrole@rGO (PPy@rGO, 8.9 mWh/cm^3) [20], as well as commercially available supercapacitors and Li thin-film batteries (Table S1 in Supporting information). Meanwhile, mPDG-LMSCs possess high areal and volumetric power densities of 424.6 μW/cm^2 and 1061.5 mW/cm^3, respectively.

The admirable electrochemical performance of mPDG-LMSCs is attributed to the controllable synthesis of mPDG heterostructures and the effective utilization of WIS gel electrolyte. First, 2D mPDG heterostructures as active materials not only couple the advantages of mesoporous materials and 2D materials, but also combine the high pseudocapacitance of PDA with the excellent conductivity and stability of graphene, ensuring high capacitance of MSCs. Second, mPDG-2 with fully exposed mesopores provides unimpeded ion-electron transfer and adaptable volume expansion in charge-discharge process, greatly enhancing the rate performance and cycle life of devices. Last but not least, the WIS gel electrolyte of SiO_2-LiTFSI endows high operating voltage, robust interfacial coupling of electrolyte and microelectrodes, and ultimately enhanced energy density and mechanical flexibility of the as-prepared planar MSCs.

In summary, we have demonstrated 2D mPDG heterostructures with well-defined mesopores and tunable thickness for safe, high-energy planar MSCs. Using GO and silica nanospheres as 2D and mesopore templates, the sheet thickness and mesopore structure of mPDG can be accurately regulated by changing the amount of DA. Particularly, the prepared mPDG-2 reveals remarkable specific mass capacitance (419 F/g at 0.5 A/g) and long cycle life (~96% retention over 5000 cycles). With mPDG-2 as active material, the mPDG-HMSCs exhibit outstanding volumetric capacitance (34.3 F/cm^3) and energy density (3.1 mWh/cm^3). More importantly, the mPDG-LMSCs with WIS gel electrolyte offer a large operating voltage of 1.6 V, as well as an amazing volumetric energy density of 11.5 mWh/cm^3, surpassing most recently reported symmetric MSCs and comparable to some asymmetric MSCs. Further, the extraordinary flexibility and self-integration capability of mPDG-HMSCs and mPDG-LMSCs endow them with great potential for flexible microelectronic applications. Therefore, this work offers many possibilities for the precise fabrication of 2D mesoporous heterostructures for high-performance MSCs.

Declaration of competing interest

The authors declare that they have no known competing financial interests or personal relationships that could have appeared to influence the work reported in this paper.

Acknowledgments

This work was supported by the National Natural Science Foundation of China (Nos. 22109040, 22125903, 22279137), Top-Notch Talent Program of Henan Agricultural University (No. 30500947), the "Transformational Technologies for Clean Energy and Demonstration" Strategic Priority Research Program of the Chinese Academy of Sciences (No. XDA21000000), DICP (No. DICP I202032), Dalian National Laboratory for Clean Energy (DNL), CAS, DNL Cooperation Fund, CAS (Nos. DNL202016, DNL202019), International Postdoctoral Exchange Fellowship Program (Talent-Introduction Program) (No. YJ20210311), China Postdoctoral Science Foundation (No. 2021M703145), the Joint Fund of the Yulin University and the Dalian National Laboratory for Clean Energy (Nos. YLU-DNL Fund 2021002, YLU-DNL Fund 2021009).

Supplementary materials

Supplementary material associated with this article can be found, in the online version, at doi:10.1016/j.cclet.2023.108845.

References

[1] M. Beidaghi, Y. Gogotsi, Energy Environ. Sci. 7 (2014) 867.
[2] S. Zheng, X. Shi, P. Das, et al., Adv. Mater. 31 (2019) 1900583.
[3] S. Bi, H. Cao, R. Wang, et al., J. Energy Chem. 63 (2021) 25–39.
[4] F. Liu, X. Feng, Z.S. Wu, J. Energy Chem. 76 (2023) 459–461.
[5] K. Chen, X. Li, J. Zang, et al., Nanoscale 13 (2021) 12370–12378.
[6] N.A. Kyerematen, T. Brousse, D. Pech, Nat. Nanotechnol. 12 (2017) 7–15.
[7] J. Zhang, G. Zhang, T. Zhou, et al., Adv. Funct. Mater. 30 (2020) 1910000.
[8] S. Wang, J. Ma, X. Shi, et al., Nano Res. Energy 1 (2022) e9120018.
[9] Z.S. Wu, X.L. Feng, H.M. Cheng, Natl. Sci. Rev. 1 (2014) 277–292.
[10] Y. Da, J. Liu, L. Zhou, et al., Adv. Mater. 31 (2019) e1802793.
[11] S. Dai, Z. Liu, B. Zhao, et al., J. Power Source. 387 (2018) 43–48.
[12] G. Moreno-Fernández, J.L. Gómez-Urbano, M. Enterría, et al., J. Mater. Chem. A 7 (2019) 14646–14655.
[13] J. Liang, A.K. Mondal, D.W. Wang, et al., Adv. Mater. Technol. 4 (2018) 1800200.
[14] J. Qin, Z.S. Wu, F. Zhou, et al., Chin. Chem. Lett. 29 (2018) 582–586.
[15] R. Chen, M. Yu, R.P. Sahu, et al., Adv. Energy Mater. 10 (2020) 1903848.
[16] C. Jing, B. Dong, Y. Zhang, Energy Environ. Mater. 3 (2020) 346–379.
[17] D. Vikraman, K. Karuppasamy, S. Hussain, et al., Compos. Part B: Eng. 161 (2019) 555–563.
[18] S.E. Moosavifard, J. Shamsi, M.K. Altafi, et al., Chem. Commun. 52 (2016) 13140–13143.
[19] Y. Shi, L. Peng, Y. Ding, et al., Chem. Soc. Rev. 44 (2015) 6684–6696.
[20] L. Chi, S. Zheng, J. Ma, et al., Carbon 194 (2022) 240–247.
[21] M. Tahir, L. He, W. Yang, et al., J. Energy Chem. 49 (2020) 224–232.
[22] H. Lee, T. Han, K.Y. Cho, et al., ACS Appl. Mater. Interfaces 8 (2016) 21366–21372.
[23] T. Liu, K.C. Kim, B. Lee, et al., Energy Environ. Sci. 10 (2017) 205–215.
[24] K. Qu, Y. Wang, A. Vasileff, et al., J. Mater. Chem. A 6 (2018) 21827–21846.
[25] X. Yue, H. Liu, P. Liu, Chem. Commun. 55 (2019) 1647–1650.
[26] T. Liu, K.C. Kim, R. Kavian, et al., Chem. Mater. 27 (2015) 3291–3298.
[27] P.J. Kim, V.G. Pol, Adv. Energy Mater. 8 (2018) 1802665.
[28] T. Liu, B. Lee, B.G. Kim, et al., Small 14 (2018) e1801236.
[29] J. Qin, H. Shi, K. Huang, et al., Nat. Commun. 12 (2021) 5786.
[30] S. Jiang, F. Xing, J. Zhang, et al., Chem. Eng. J. 452 (2023) 139095.
[31] Y. Yan, G. Chen, P. She, et al., Adv. Mater. 32 (2020) e2004654.
[32] A.E. Allah, J. Wang, Y.V. Kaneti, et al., Nano Energy 65 (2019) 103991.
[33] R. Zhang, H. An, Z. Li, et al., Chem. Eng. J. 289 (2016) 85–92.
[34] Y. Zhu, S. Murali, W. Cai, et al., Adv. Mater. 22 (2010) 3906–3924.
[35] Z. Li, S. Wu, W. Lv, et al., Small 12 (2016) 2674–2688.
[36] T. Liu, B. Lee, B.G. Kim, et al., Small 14 (2018) 1801236.
[37] S. Liu, P. Gordiichuk, Z.S. Wu, et al., Nat. Commun. 6 (2015) 8817.
[38] Y. Song, T.Y. Liu, X.X. Xu, et al., Adv. Funct. Mater. 25 (2015) 4626–4632.
[39] Q. Wu, T. He, Y. Zhang, et al., J. Mater. Chem. A 9 (2021) 24094–24147.
[40] H. Xiao, Z.S. Wu, L. Chen, et al., ACS Nano 11 (2017) 7284–7292.
[41] F. Zhou, H. Huang, C. Xiao, et al., J. Am. Chem. Soc. 140 (2018) 8198–8205.
[42] J. Qin, S. Wang, F. Zhou, et al., Energy Storage Mater. 18 (2019) 397–404.
[43] B. Song, L. Li, Z. Lin, et al., Nano Energy 16 (2015) 470–478.
[44] W. Gao, N. Singh, L. Song, et al., Nat. Nanotechnol. 6 (2011) 496–500.
[45] M. Beidaghi, C. Wang, Adv. Funct. Mater. 22 (2012) 4501–4510.
[46] M.F. El-Kady, R.B. Kaner, Nat. Commun. 4 (2013) 1475.
[47] S. Zheng, Z.S. Wu, S. Wang, et al., Energy Storage Mater. 6 (2017) 70–97.
[48] Y. Zhu, S. Zheng, J. Qin, et al., Fund. Res. 4 (2024) 307–314.
[49] Y. Zhu, S. Zheng, P. Lu, et al., Natl. Sci. Rev. 9 (2022) nwac024.
[50] H. Tian, J. Qin, D. Hou, et al., Angew. Chem. Int. Ed. 58 (2019) 10173–10178.
[51] J. Qin, F. Zhou, H. Xiao, et al., Sci. China Mater. 61 (2018) 233–242.
[52] J. Qin, J. Gao, X. Shi, et al., Adv. Funct. Mater. 30 (2020) 1909756.